IEEE Access
Multidisciplinary | Rapid Review | Open Access Journal

Received June 9, 2019, accepted July 18, 2019, date of publication July 23, 2019, date of current version August 12, 2019.

Digital Object Identifier 10.1109/ACCESS.2019.2930680

State of Health Estimation for Lithium-ion Batteries Based on Fusion of Autoregressive Moving Average Model and Elman Neural Network

ZHENG CHEN[1], (Senior Member, IEEE), QIAO XUE[1], RENXIN XIAO[1], YONGGANG LIU[2], (Senior Member, IEEE), AND JIANGWEI SHEN[1]

[1]Faculty of Transportation Engineering, Kunming University of Science and Technology, Kunming 650500, China
[2]State Key Laboratory of Mechanical Transmissions, School of Automotive Engineering, Chongqing University, Chongqing 400044, China

Corresponding authors: Yonggang Liu (andyliuyg@cqu.edu.cn) and Jiangwei Shen (shenjiangwei6@163.com)

This work was supported in part by the National Science Foundation under Grant 61763021 and Grant 51775063, in part by the National Key Research and Development Program of China under Grant 2018YFB0104500, and in part by the EU-funded Marie Skłodowska-Curie Individual Fellowships Project under Grant 845102-HOEMEV-H2020-MSCA-IF-2018.

ABSTRACT This paper proposes a fusion model based on the autoregressive moving average (ARMA) model and Elman neural network (NN) to achieve accurate prediction for the state of health (SOH) of lithium-ion batteries. First, the voltage and capacity degradation variation of the battery are acquired through the battery lifecycle data, and the health factor related to the battery aging is selected according to the variation of the voltage profile. Second, the empirical mode decomposition (EMD) is employed to process the capacity degradation data and eliminate the phenomenon of tiny capacity recovery, and multiple data sequences, as well as the related residue, are extracted, then the grey relational analysis (GRA) between sub-sequences and health factor are discussed. Furthermore, the ARMA model and Elman NN model are respectively built by training the subsequent time series data and residue data. Finally, all the individual predictions are combined to generate the estimated SOH sequences. The experimental validation is performed to manifest that the addressed fusion method performs the SOH prediction with satisfactory accuracy, compared with the single ARMA method and Elman NN model.

INDEX TERMS Autoregressive moving average (ARMA), Elman neural network (NN), grey relational analysis (GRA), empirical mode decomposition (EMD), state of health (SOH).

NOMENCLATURE

A. ABBREVIATIONS

ARMA	autoregressive moving average
NN	neural network
SOH	state of health
EMD	empirical mode decomposition
GRA	grey relational analysis
EVs	electric vehicles
HEVs	hybrid electric vehicles
BMS	battery management system
SOC	state of charge
ECM	equivalent circuit models
SEI	solid electrolyte interphase
SVM	support vector machine
GPR	Gaussian process regression
PF	particle filter
RFR	random forest regression
IC	incremental capacity
CVCAF	constant voltage charging aging factor
OCV	open circuit voltage
PCA	principal component analysis
RVM	relation vector machine
RUL	remaining useful life
EIS	electrochemical impedance spectroscopy
IMF	intrinsic mode function
CC	constant current
Ah	Ampere-hour
CV	constant voltage
AR	autoregressive model

The associate editor coordinating the review of this manuscript and approving it for publication was Mouloud Denai.

MA	moving average model
AIC	Akaike information criterion
MSE	mean-square error
MARE	mean-absolute-relative error

B. SYMBOLS

C_u	the present capacity of the battery
C_r	the rated capacity of the battery
$x(t)$	time series
$U(t)$	upper envelope of $x(t)$
$L(t)$	lower envelope of $x(t)$
$m(t)$	the average envelope of the upper and lower envelopes
$h(t)$	the pending IMF
$r_n(t)$	residue of the $x(t)$
T	the number of original data points the number of iterations in the decomposition process
SD	the termination parameter
F_1	CC mode duration
$y(k)$	reference series correlation grade the autoregressive model parameter
p	the order of the AR model the moving average model parameter
q	the order of the MA model
B	backward shift operator
L	the highest order of the ARMA model
ε_t	the residual of the ARMA model
τ	the condition for validating the residual independence of the model the m-dimensional output vector
x	the n-dimensional mid-layer element vector
u	the r-dimensional input vector
x_c	n-dimensional feedback state vector
ω^3	the weight matrix between the middle layer and output layer
ω^2	the weight matrix between the input layer and middle layer
ω^1	the weight matrix between the context layer and middle layer
g	the transfer function of the output neuron
f	the transfer function of neurons in the middle layer.
η_1	the learning rates of ω^1
η_2	the learning rates of ω^2
η_3	the learning rates of ω^3

I. INTRODUCTION

With the development of the world economy and increase of population, the energy demand keeps increasing. Due to continuous consumption of non-renewable energy such as fossil energy and gradual deterioration of environmental pollution, the development of environmentally friendly renewable energy has attracted much attention [1], [2]. Nowadays, lithium-ion batteries have been widely applied in electric vehicles (EVs) and hybrid electric vehicles (HEVs) because of their advantages of high energy density, no memory effect, low self-discharge rate and environmental protection [3]. Nowadays, lithium-ion battery packs occupy a high proportion in the whole vehicle cost. For the sake of economic benefits and safety, it is imperative to manage the battery pack operating properly, so as to provide decision-making reference for the maintenance and life prediction of the battery pack. In actual operation, the electrode material of the lithium-ion battery gradually becomes inactive with accumulated operation. Meanwhile, the inner structure of physics and the associated chemical reaction would change, resulting in the capacity attenuation [4]. Consequently, the state of health (SOH) is introduced which characterizes the healthy status of lithium-ion batteries. In the battery management system (BMS) of EVs and HEVs, the SOH is a nonrepresentational definition with no specific quantitative index. Generally, the capacity attenuation of the battery is taken as the main measurement index of the battery SOH. Accurate estimation of the SOH can make an essential contribution to battery health management, including avoiding catastrophic hazards and extending the battery lifespan [5]. However, due to complexity and strong coupling of the internal electrochemical reactions of the battery, to the authors' best knowledge, there is still not comprehensive and clear explanation of the mechanism of battery degradation. In addition, different types of lithium-ion batteries lead to different aging mechanisms due to various inner structure design and electrode materials [6]. As such, accurate prediction of the health status of the battery still poses considerable challenges.

The battery degradation is an irreversible process, and the improper operating temperature, overcharge, over-discharge and other unhealthy usage habits will accelerate the aging of the battery. Due to the obscure internal dynamic chemical system and sensitivity to external environmental factors of lithium-ion batteries, it is difficult to identify their degradation mechanism [7]. When the capacity drops to 80% of the initial value, it is deemed unfit for vehicular applications and the battery should be replaced, since when the available capacity drops less than 80% of the rated capacity, the capacity degradation will then show an exponential decline trend with even faster dropping speed [8]. In view of these problems, how to accurately estimate the healthy status of batteries shows significance on the BMS of EVs. Meanwhile, accurately predicting the SOH is also critical for estimating other status of the battery. If the SOH of the battery can be accurately estimated, the SOC estimation accuracy can be potentially improved. In addition, if the battery SOH can be estimated timely and accurately, the present battery available capacity can be provided to the BMS for the balance control. Previous studies have shown that elements related to the aging rate of the battery, such as charging and discharging rate, depth of discharge and ambient storage conditions, can influence the operating state of the battery [9]. If more information with respect to aging of battery can be acquired, the service lifespan can be extended and safety accidents can

be avoided to some extent [10], [11]. Nowadays, a variety of methods have been proposed to predict the battery SOH, which can be roughly divided into three categories [12]: empirical based methods, model-based methods and data-driven methods.

Empirical based methods are applied to estimate the SOH by fitting the empirical data. This kind of methods can meet a certain prediction accuracy for a specific battery, however it needs to be implemented under certain conditions. When the battery is faced with complex and variable operating conditions, it is difficult to achieve accurate estimation by this manner [13]. In practice, it can only be used as rough estimation of the SOH. Model-based methods, representing a key direction of investigating battery degradation, conduct the SOH estimation by means of establishing a battery model and identifying variation of the interrelated parameters. Electro-chemical models, equivalent circuit models (ECM) and empirical degradation models are mostly widely adopted [14]–[16]. The electro-chemical model analyzes operation law of the battery during degradation from the electrochemical perspective, and it needs to fully consider influence of the battery voltage, current, diffusion coefficient, temperature, and electrolyte concentration. In [16], an integrated chemical and physical decay mechanism is proposed to predict the battery SOH, in which the variation of chemical and physical structures of positive and negative electrodes are analyzed in detail. Experimental results show that the internal structure of the battery is cracked and expanded, and a solid electrolyte interphase (SEI) layer is generated on the new cracked surface, leading to decline of the battery capacity. For this method, even it shows a high prediction accuracy, however, it requires a variety of derivation and calculation. The model-based method can well reflect the physical and chemical characteristics of the battery; nonetheless, the accuracy and stability of the model can greatly depend on selection of the parameters [17]. The data-driven method does not take complex physical and chemical reactions inside the battery into account, but instead directly tracks the battery health variation based on the collected operation data, by which the SOH can be estimated [18], [19] An important advantage of the data-driven method is that investigators do not need to model the mechanism characteristics of the degradation. In contrast, it only needs to apply the machine learning algorithm or an oriented data analysis method to build a black-box model with input of electrical measurements and output of SOH. Typical data-driven methods include the support vector machine (SVM) algorithm [20], [21], neural networks (NNs) [22], Gaussian process regression (GPR) [23], particle filter (PF) [24], and random forest regression (RFR) [25]. In [20], based on the characteristics of charging voltage curve, the SVM model with different voltage range is established, and then the grid search algorithm based on cross-validation is adopted to optimize the model parameters, so as to find the optimal voltage range for SOH prediction. In [11], [13], relevant feature vectors are extracted according to the variation characteristics of incremental capacity (IC) curve, and then the GPR is employed to estimate the SOH of the battery. In [26], the constant voltage charging aging factor (CVCAF) is regarded as the measurement index to achieve precise estimation of the battery SOH without full cycle experiment. In [27], a total of 14 features are extracted and analyzed by the grey relational analysis (GRA) and principal component analysis (PCA), and then the relation vector machine (RVM) is leveraged for further prediction. In [28], a data-driven method is combined with large amount of data to predict the cycle life for batteries before degradation occurs. In [29], a fusion of IC analysis and GPR algorithm is leveraged to integrate the SOH estimation and RUL prediction. While the data-driven method does not need to consider the degradation mechanism of the battery in depth, sufficient effective offline data should be collected to train the estimation model. The estimation accuracy is also fragile when facing with uncertainty and limited range of the original data [30]. Moreover, these data-driven methods are limited by computational intensity of the BMS and not easy to implement in real application [31].

To address the above elaborated problems and achieve accurate SOH prediction, some characteristic changes during the aging process need to be carefully considered. For instance, the capacity recovery phenomenon possibly occurs in the process of battery degradation, especially when some intervals exist under the condition that the battery is cycled with full charge and discharge operation. This local tiny capacity recovery indicates that the battery capacity degradation does not monotonously decline with the increase of cycle number. It may change the local variation trend of the SOH and thus affect the prediction accuracy [32]. In terms of the model-based and data-driven methods discussed above, one or more health indicators such as capacity and impedance are extracted as the model inputs to increase the prediction accuracy of SOH [33]. For example, the capacity decay model and electrochemical impedance spectroscopy (EIS) are often employed to predict the SOH [34], [35]. The battery capacity is usually measured and calculated in a complete cycle operation under specific conditions. In actual operation, it is difficult to encounter a full cycle operation [33]. Meanwhile, the battery impedance cannot be directly and accurately measured online by conventional sensors of the electrical system, hindering its online application [36]. Considering difficulties in application of capacity and impedance measurement in practical operation, indirect health indicators are considered for the SOH prediction. Although they do not directly relate to the SOH, they show great correlation with the capacity variation during the whole life cycle. Typical candidates include IC [11] and differential voltage analysis [37]. No doubt, they are more intelligible and direct to capture the capacity variation, compared with the capacity and impedance measurement methods. As such, if some indirect health indicators that have a certain degree of correlation with SOH can be extracted without complex experiment and modeling process, it would become easier to conduct the estimation.

Based on the above analysis, the priority of this paper is to attain estimating the battery SOH with high accuracy, acceptable calculation intensity and strong stability by selecting proper health indicators. Considering phenomenon of tiny capacity recovery during the battery lifecycle experiment, the empirical mode decomposition (EMD) technology is employed to process the raw SOH data sequence. Then, taking into account changes in the voltage curve during the attenuation of battery capacity, an indirect healthy factor that shows a certain degree of correlation with SOH is extracted, so as to enhance the prediction reliability and improve the accuracy. In this study, the grey relational analysis (GRA) is applied to determine the correlation grade among the EMD decomposition results, cycle number and health factor. Furthermore, different correlation grade shown in the analysis results is harnessed for subsequent prediction by the autoregressive moving average (ARMA) model and Elman NN model. Experimental results prove feasibility of the proposed method. The main contribution of the study can be attributed to the following three aspects:

1) The EMD is employed to process local variation of the raw SOH data, and thus the local capacity recovery phenomenon can be fully considered. After decomposition, three intrinsic mode functions (IMFs) along with the residue can be attained.
2) The duration of the constant current charging process is considered as the health indicator by analyzing the battery charging data, and the health indicator is correlated with the IMFs and its residue with help of the GRA.
3) The ARMA model and Elman NN are respectively employed to predict the IMFs and residue, and the SOH prediction is conducted by incorporating both estimation results. The proposed ARMA-Elman NN model can fully consider the local tiny capacity recovery and the complex information variation during the charging process, thereby achieving the reliable and precise SOH estimation.

The remainder of this paper is structured as follows. In Section II, the battery attenuation experiment is introduced, and related data analysis is conducted. In Section III, the EMD and GRA are employed to deal with the experimental data and extract the health factor. In Section IV, the ARMA model and Elman NN model are introduced in detail. In Section V, a series of predicted results are discussed, and the final SOH estimation is performed by incorporating two algorithms' result, followed by main conclusions drawn in Section VI.

II. BATTERY CYCLE LIFE ATTENUATION EXPERIMENT AND AGING FEATURES EXTRACTION

A. DEFINITION OF STATE OF HEALTH

In this study, the current health status of an aged battery is determined according to the specific performance compared with its initial value [38]. In this paper, we define the SOH according to the percentage of available capacity over the rated value, as:

$$SOH = \frac{C_u}{C_r} \times 100\% \tag{1}$$

where C_u and C_r denote the present capacity and rated capacity of the battery, respectively.

B. EXPERIMENT AND DATA ANALYSIS

In this paper, five lithium-ion batteries (referred to as Cells 1 to 5 hereinafter) were experimented on. They belong to two types of batteries, of which one type (Cells 1, 3 and 4) is 21700-size with anode materials of Li(NiCoMn)O2, and the other type (Cells 2 and 5) is the 18650-size with anode materials of LiCoO2. They are with different electrode materials and cell structures, and show different performances in energy density, power capability and self-discharge rate. Certainly, their degradation performances are different. During experiment, three operation states exist including the charging process, discharging process and rest. Related parameters of two batteries are shown in TABLE 1.

TABLE 1. Related parameters of Cell 1 and Cell 2.

Item	Parameters	
	Cell 1	Cell 2
Nominal capacity	4Ah	2.55Ah
Charge mode	CC/CV	CC/CV
Charge limited voltage	4.2V	4.2V
Charge cut-off current	80mA	51mA
Discharge cut-off voltage	2.75V	2.5V

According to the test process, the experimental scheme for the battery cycle life attenuation is designed as follows:

1) The battery is subjected to constant current (CC) charge of 0.5C (Cell 1) and 1C (Cell 2) at 25ř until the terminal voltage reaches its upper limit. Here, C denotes the value of the battery nominal capacity with unit Ampere-hour (Ah).
2) Then, the battery is charged under the constant voltage (CV) mode until the current drops to the cut-off threshold.
3) Consequently, the battery is kept still for 1 hour.
4) Next, the battery is discharged with the current of 3C (Cell 1) and 2C (Cell 2) until the battery voltage drops to the allowable cut-off values.
5) Repeat steps 1) to 4) to conduct cycling experiment.

The current and voltage profiles during one cycle are shown in Fig. 1. As can be seen, the charging process is divided into the CC and CV modes, and the discharging process only includes the CC mode. The full charging voltage of two cells is 4.2V and the discharging cut-off voltage is different, one is 2.75V and the other one is 2.5V.

The relationship between the capacity attenuation and the cycle number is depicted in Fig. 2. As can be found, there exists a local tiny capacity restoration that occurs in the cycling process. This is due to a certain experiment interval

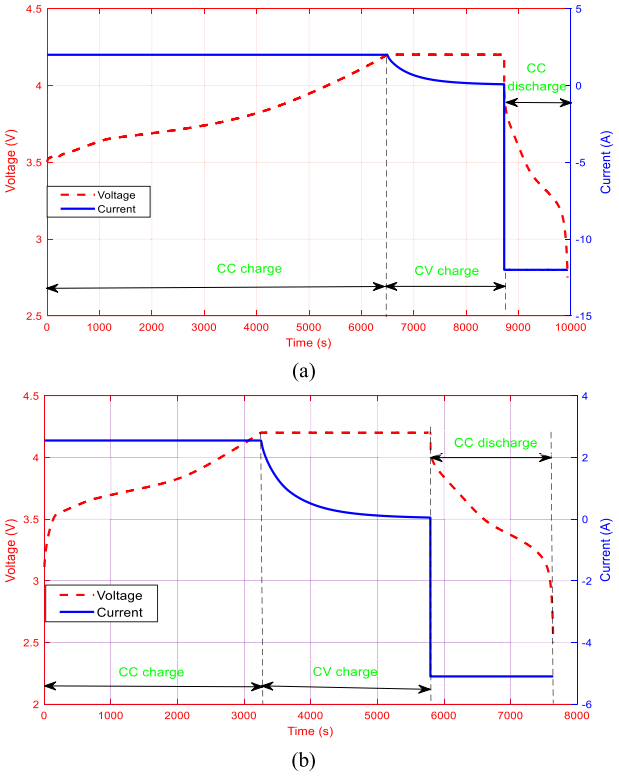

FIGURE 1. Charge and discharge cycle experiment of battery cells.

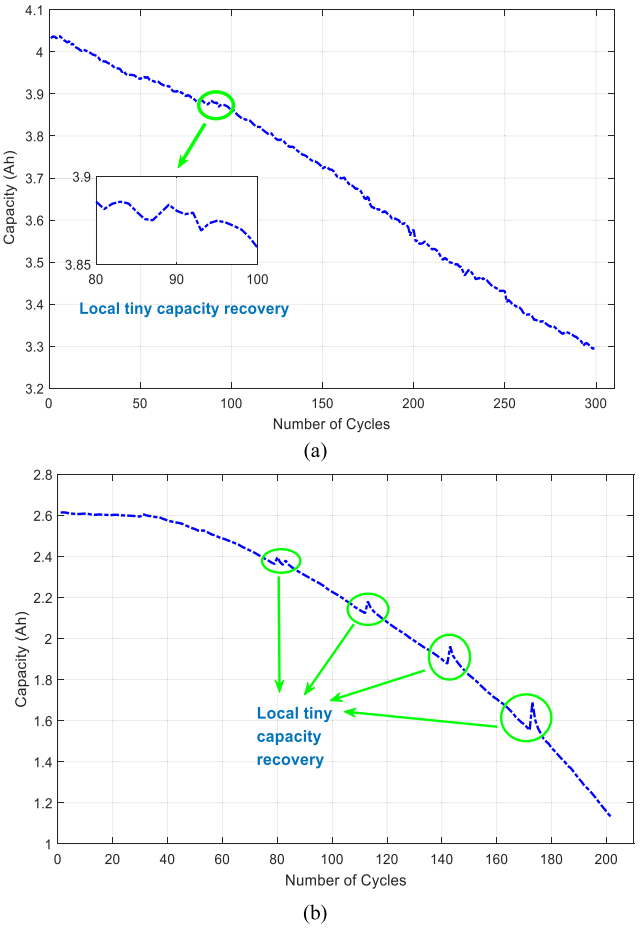

FIGURE 2. Capacity degradation curve of Cell 1 (a) and Cell 2 (b).

that leads to partial recovery of the battery capacity. However, this local tiny capacity regeneration phenomenon takes a certain impact on the SOH estimation. In order to reflect the local information change of SOH caused by the tiny recovery of the battery capacity, and accurately predict the battery SOH, the EMD algorithm is applied to decompose the SOH variation signal into several intrinsic mode functions (IMFs). It contains local characteristic values of the original signal with different time scales, which enables that local small change can be properly dealt with for the SOH estimation.

C. HEALTH FACTOR EXTRACTION AND ANALYSIS

With the increase of the cycle number, some significant changes would occur in the charge and discharge duration of the battery. These changes are related with degradation of the battery and can imply the battery health variation to some extent. Taking Cell 1 as an example, the charging voltage curves at partial cycles are shown in Fig. 3(a), where we can find that the duration of CC charge mode decreases with the cycling operation. The duration directly affects that how much capacity can be charged in the CC mode, which represents the battery polarization characteristics to some extent. With aging of the battery, the polarization phenomenon will gradually exacerbate, leading to decrease of the CC mode duration. In actual operation process, it is difficult to directly know the residual capacity and the use condition of the battery. If the past charging data can be analyzed to find the CC charging duration as well as the hidden relationship with respect to the battery SOH, then knowing the CC duration can be beneficial to estimation of the battery SOH. On this account, the CC mode duration shown in Fig. 3(b) is extracted as a health factor which is denoted as F1. In order to facilitate further analysis and comparison, F1 is normalized. Fig. 4 shows the variation trend of F1 and SOH of Cell 1 with the increase of cycle numbers.

In the next step, data processing and analysis are conducted according to the health indicator and the proposed method.

III. DATA PROCESSING AND ANALYSIS

As introduced before, the EMD technique is applied to decompose the experimental data.

A. EMPIRICAL MODE DECOMPOSITION

EMD is a time series data or signal processing technology proposed in [39], [40], which can extract the oscillation modes of different frequency features embedded in the signal or time series without knowing the data stationary and nonlinear characteristics. During the decomposition process, EMD should satisfy the following criteria: 1) in the whole data set, the quantity of local extremum points should be

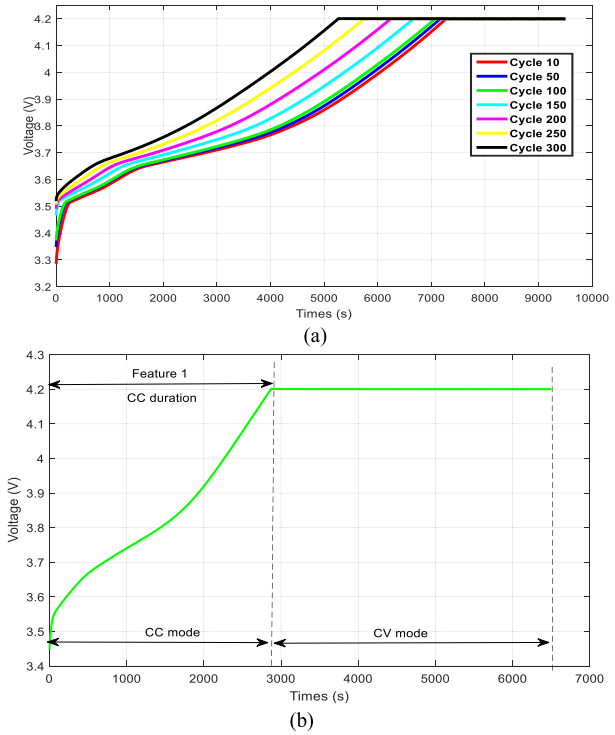

FIGURE 3. (a) Charging voltage curves of Cell 1 at different cycles. (b) The health factor selection based on charging curve.

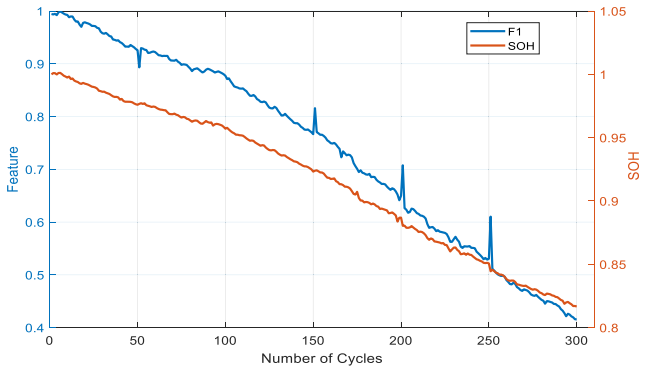

FIGURE 4. Changes of F 1 and SOH with cycle numbers.

equal to or at most be only one difference from the number of zero points; and 2) at any time, the mean value of the upper envelope defined by the local maximum value and the lower envelope defined by the local minimum value should be zero. The EMD algorithm mainly extracts IMFs by filtering the inputs [39], which can be illustrated as follows:

1) Discern partial extremum values of the time series $x(t)$.
2) Fit the upper envelope $U(t)$ and the lower envelope $L(t)$ of $x(t)$ by the cubic spline interpolation method based on all of local extreme values.
3) Calculate the average envelope $m(t)$ of the upper and lower envelopes,

$$m(t) = [U(t) + L(t)]/2 \tag{2}$$

4) Subtract the mean envelope $m(t)$ from to extract the pending IMF,

$$h(t) = x(t) - m(t) \tag{3}$$

5) Determine whether $h(t)$ meets the criteria of the IMF mentioned above or not. If not, replace $x(t)$ with $h(t)$ and repeat screening from step 1); otherwise, $h(t)$ is regarded as the IMF, as shown in (4). Then turn to step 1) to continue screening by replacing with the residue $r(t)$.

$$c_i(t) = h(t) \tag{4}$$
$$r(t) = x(t) - h(t) \tag{5}$$

6) Repeat steps 1) to 5) until the termination criteria is reached. The decomposition results can be described as:

$$\begin{cases} r_n(t) = x(t) - \sum_{i=1}^{n} c_i(t) \\ r_i(t) = r_{i-1} - c_i(t) \end{cases} \tag{6}$$

where $r_n(t)$ denotes the residue and is a monotonous function representing the trend of data series.

It can be indicated that the stopping criteria employed in step 6) can be expressed as:

$$SD = \sum_{t=0}^{T} \frac{|h_{(k-1)}(t) - h_k(t)|^2}{h^2_{(k-1)}(t)} \tag{7}$$

where T represents the quantity of original data points, k means the iterations of the decomposition, and SD denotes the termination parameter. SD is determined specifically according to actual complexity of the signal contained in the time series data [41]. In this study, based on repeated iterations of the experimental data of Cell 1, the decomposition is stopped when $SD \leq 0.05$, and for Cell 2, it is that $SD \leq 0.08$. The results of EMD decomposition of the two cells' data are shown in Figs. 5 and 6, respectively. The SOH sequences of Cell 1 and Cell 2 are both decomposed into 3 IMFs together with a residue. It can be seen that the decomposition results with three IMFs show high fluctuation frequency, and the final residue is a smooth monotone curve that represents the SOH variation trend, validating feasibility of the EMD algorithm.

B. CORRELATION DEGREE ANALYSIS BASED ON GRA

The SOH sequences of Cell 1 and Cell 2 are both decomposed by the EMD to obtain three IMFs and a residue. IMFs represents the oscillation mode of SOH series in different time scales, whereas the residue explains the variation trend of SOH in the whole cycle life. In addition, they are also correlated with F1 to a certain extent. To better understand the implicit mapping, the GRA algorithm is applied to analyze the relationship among F1, IMFs and the residue. The GRA method is a data analysis method stemmed from grey

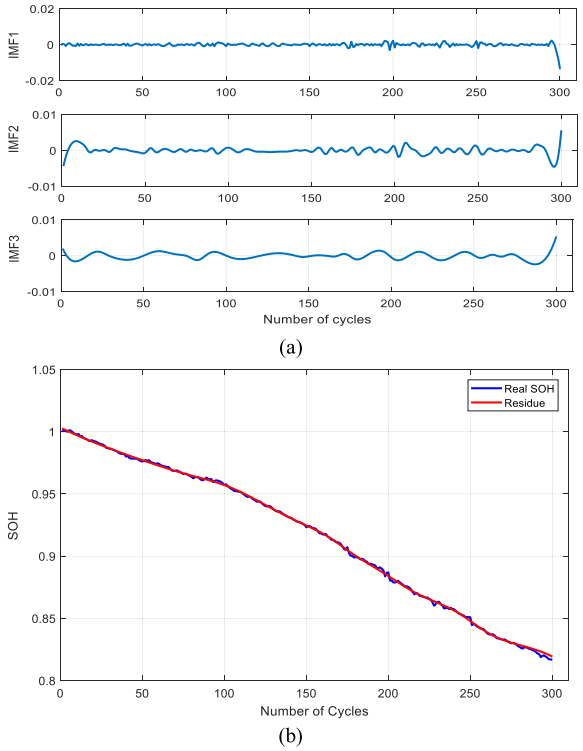

FIGURE 5. The original SOH sequence of Cell 1 was decomposed by EMD to obtain three IMFs and a residue. (a) Three IMFs; (b) The residue.

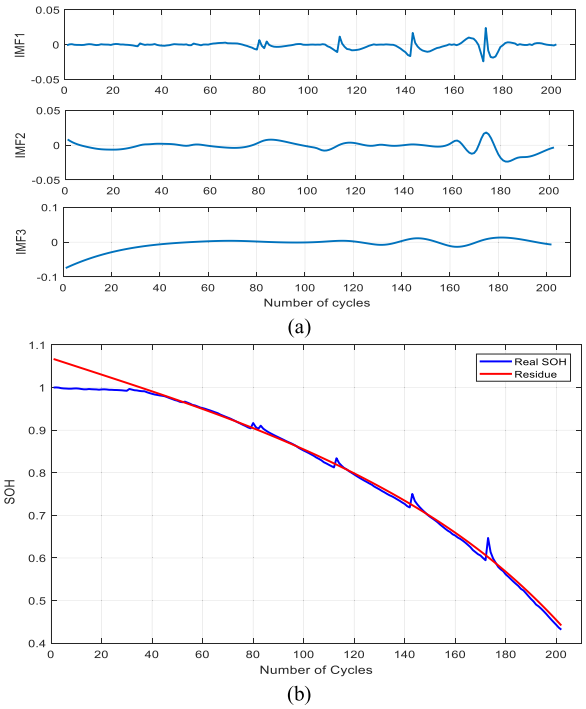

FIGURE 6. The original SOH sequence of Cell 2 was decomposed by EMD to obtain 3 IMFs (a) and a residue (b).

system theory and measures the relational grade among factors according to similarity or dissimilarity of the development trends among factors. It provides quantitative analysis to highlight the similarity and difference between reference sequences and comparison sequence [42]. The implementation of the GRA is detailed as follows:

1) Determine the reference $y(k)$ and actual values $x(k)$ for the given data. In this paper, the reference series are IMFs and residue, i.e., $y(k) =$ [IMF1 IMF2 IMF3 residue] and $x(k) = F_1(k)$.
2) Nondimensionalize the data series.
3) Calculate the absolute difference sequence and find the maximum and minimum values, where the absolute difference is the absolute value of the difference between the reference and comparison series, as

$$\begin{cases} \Delta_{ij}(k) = \left| y_i(k) - x_j(k) \right| \\ A = \min \Delta_{ij}(k) \\ B = \max \Delta_{ij}(k) \end{cases} \tag{8}$$

4) Calculate the correlation coefficient $\xi_{ij}(k)$, as:

$$\xi_{ij}(k) = \frac{A + \rho B}{\Delta_{ij}(k) + \rho B} \tag{9}$$

where $\rho \in (0, 1)$ means the resolution coefficient. In this paper, $\rho = 0.5$.
5) Calculate the correlation grade, as:

$$r_{ij} = \sum_{k=1}^{n} \xi_{ij}(k) \tag{10}$$

The calculation results of the correlation grade are shown in Tables 2 and 3, respectively.

TABLE 2. Grey relational grades between F1 and SOH.

Battery Number	Item			
	IMF1	IMF2	IMF3	Residue
Cell 1	0.4163	0.4155	0.4166	0.7550
Cell 2	0.4663	0.4656	0.4880	0.6887

TABLE 3. Grey relational grades between cycles and SOH.

Battery Number	Item			
	IMF1	IMF2	IMF3	Residue
Cell 1	0.5529	0.5536	0.5507	0.5944
Cell 2	0.5503	0.5508	0.6223	0.5825

We can find the correlation grade between F1 and IMFs is only 0.4, and the degree of correlation is small. The correlation grade between F1 and the residue of Cell 1 and Cell 2 are 0.7550 and 0.6887, respectively. We can conclude that F1 shows a greater correlation grade with the residue; therefore, when the prediction of the residue is performed, the feature factor F1 can be added as the model input.

IV. ALGORITHM AND PREDICTION MODEL

A. SELECTION OF MODEL AND PREDICTION PROCESS

According to the above analysis, IMFs and the residue show different correlation degrees with F1. The IMFs has little correlation grade with F1 and shows a certain grade of correlation with the number of cycles. From this point of view, IMFs may have a greater correlation grade with the observed values in the past. The IMFs are regarded as a time series, and the ARMA model is herein applied for prediction. In contrast, there is a large correlation grade between the residue and F1, and the residue exhibits a certain degree of correlation with the number of cycles. In order to reflect the implied complexity of the association without knowing the complicated relationship in much detail, the Elman NN is employed to predict the residue and the whole prediction process is shown in Fig. 7.

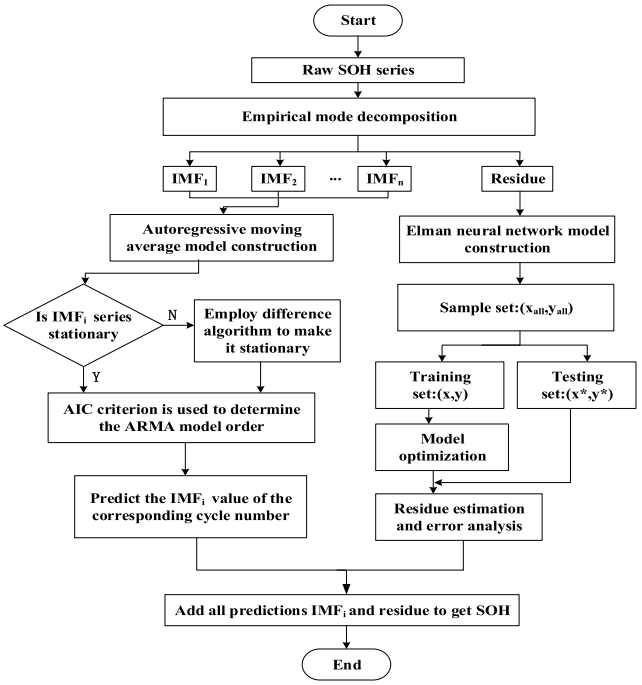

FIGURE 7. The SOH prediction procedure.

As can be seen in Fig. 7, the SOH data sequence can be decomposed into a few IMFs along with the residue. Then two different algorithms are applied to estimate the SOH based on the IMFs and residue, respectively. Among them, the ARMA algorithm is in charge of the IMF data and the Elman NN is to deal with the residue. Since the ARMA model requires high demand of the data stability, it is necessary to judge the data's variation rate in advance. As the IMFs exhibits obvious oscillation with large frequency, here a differential calculation is employed to stabilize the signal before building the ARMA model. With respect to the residue's estimation, depicted in Fig. 7, $x_{all} = [F_1\ cycle]$ represents the model input and $y_{all} = [SOH]$ is the model output. The main purpose of the model optimization is to better select learning rules of the Elman NN. To avoid the error backpropagation, the gradient descent method is employed to regulate each layer's weights and thresholds, thereby approximating the anticipated value with high precision.

B. AUTOREGRESSIVE MOVING AVERAGE MODEL

1) OVERVIEW OF THE ARMA MODEL

The ARMA model can be used for regression analysis of large amounts of data and short-term prediction [43], [44]. The ARMA model is composed of an autoregressive model (AR) and a moving average model (MA). For a stochastic process or time series observation ($X_t,\ t = 0, \pm 1$), which is related to or dependent on previous observations ($X_{t-1}, X_{t-2}, \cdots$), a random differential equation can be utilized to describe the relationship under certain assumption,

$$X_t = \varphi_1 X_{t-1} + \varphi_2 X_{t-2} + \cdots + \varphi_p X_{t-p} + a_t \tag{11}$$

where φ_j $(1 \le j \le p)$ is the autoregressive parameter, p is the order of the model, and a_t means the white noise.

The MA predicts the future value based on the linear combination of the past interference and present interference values. Its mathematical expression can be presented as:

$$X_t = a_t - \theta_1 a_{t-1} - \theta_2 a_{t-2} - \cdots - \theta_q a_{t-q} \tag{12}$$

where $\theta_j (1 \le j \le q)$ are the coefficients to be determined, and q means the order of the model. Now, the ARMA model integrating AR(p) and MA(q) can be merged as:

$$X_t - \varphi_1 X_{t-1} - \cdots - \varphi_p X_{t-p} = a_t - \theta_1 a_{t-1} - \cdots - \theta_q a_{t-q} \tag{13}$$

Applying the backward shift operator B, equation (13) can be written as:

$$\begin{cases} \varphi(B) X_t = \theta(B) a_t \\ \varphi(B) = 1 - \varphi_1 B - \varphi_2 B^2 - \cdots - \varphi_p B^p \\ \theta(B) = 1 - \theta_1 B - \theta_2 B^2 - \cdots - \theta_q B^q \end{cases} \tag{14}$$

In this study, an assumption is made that $\varphi(B)$ and $\theta(B)$ do not have common factors.

2) IDENTIFICATION OF THE ARMA MODEL

In this study, the Akaike information criterion (AIC) [45] is employed to solve p and q, and the order of the ARMA model is determined based on the AIC criterion, as expressed in (15). The calculating process of the AIC criterion is detailed as follows. First, the residual variance σ_k^2 of the model is calculated based on X, and the highest order L of the fitting model is imposed. In general, L can be $\sqrt{N}, N/10$ or $\ln N$ [46] and in this study, L is selected as $N/10$. Second, the AIC value is computed with the range of $0 \le p \le L$ and $0 \le q \le L$. Finally, different p and q are respectively evaluated, followed by the model parameter estimation. The AIC values of each model are compared, and the model with the minimum AIC value is selected as the optimal model. During the calculation process, p and q are determined as the order of the model.

$$AIC(p, q) = \log \sigma_k^2 + \frac{2(p + q + 1)}{N} \tag{15}$$

Equation (15) indicates that the AIC value is composed of two terms. The first one represents the quality of model fitting, which decreases with increment of the order. The second item characterizes the number of parameters of the model. When applying the AIC criterion, it should be noted that if the minimum point of the AIC cannot be determined by approaching the upper limit of the order, the preset upper limit should be enlarged to continue screening the parameters.

TABLE 4. Parameters (p, q) for each ARMA model.

Battery	IMF1	IMF2	IMF3
Cell 1	4, 4	6, 3	11, 12
Cell 2	1, 2	4, 3	9, 9

3) ADAPTIVE VERIFICATION OF THE MODEL

In this paper, the IMFs and the associated residues acquired from the data decomposition are analyzed, and the corresponding ARMA models are established by training 60% of the data. The detailed values of p and q of the ARMA model are listed in Table 4. After establishing the ARMA model, its adaptability in terms of each IMF discussed above needs to be verified. Generally, the independence of the residual ε_t in the fitting model is applied to validate whether the model is qualified for the actual situation. According to the Barlett's formula [47], $\tau = \pm(2/\sqrt{N})$ is considered as the condition for validating the residual independence of the model, where N is the number of the training data. The autocorrelation function of the residual for IMFs are shown in Fig. 8. For Cell 1, N equals 180 and $\tau_1 = \pm 0.149$. It can be seen that most of the values of three IMFs are less than τ_1 and they all gradually converge to zero. In terms of Cell 2, $\tau_2 = \pm 0.183$, and it can be observed from Fig. 8 (b), that most of the time the other autocorrelation function values are less than τ_2 and also gradually converge to zero. Therefore, it can be inferred that ε_t of each fitting model is independent with the confidence of 5%, and thus the effectiveness of the ARMA model is validated.

C. ELMAN NN AND ITS APPLICATION

Elman NN is essentially a kind of dynamic feedback networks, which uses a context layer as a one-step delay operator to realize the function of memory, for the sake of facilitating the ability to adapt to the time-varying characteristics [48], [49]. The inner structure of the Elman NN is shown in Fig. 9. A main characteristic is that the context layer receives and stores feedback signals from the hidden layer, and each node of the hidden layer is connected with a corresponding node of the context layer, making it accessible to the data of historical state. The addition of the internal feedback network enhances the ability to process dynamic information, thereby making easier adaptation to dynamic modeling. In addition, Elman NNs can approximate arbitrary nonlinear relationship with ideal precision with more computational power, compared with feedforward NNs.

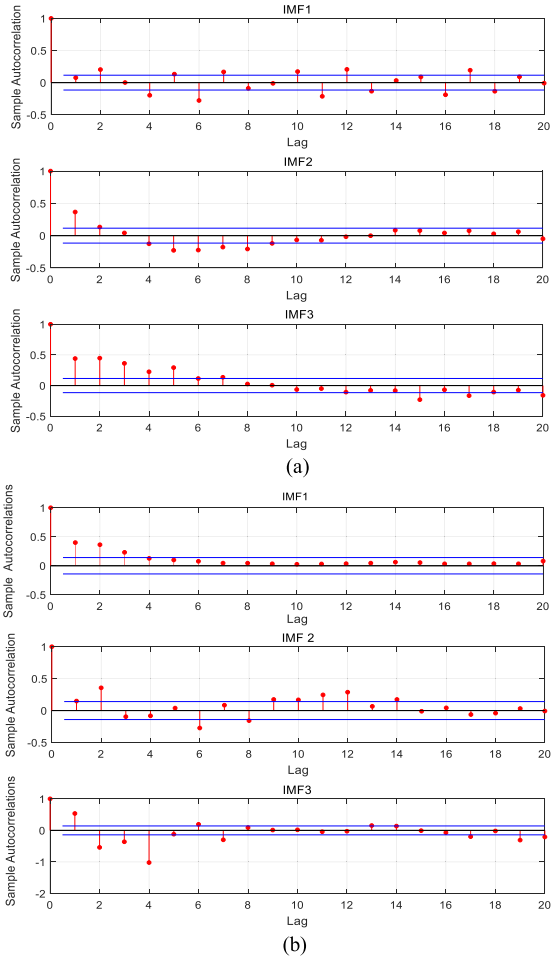

FIGURE 8. Autocorrelation diagram of residual of IMFs for Cell 1 (a) and Cell 2 (b).

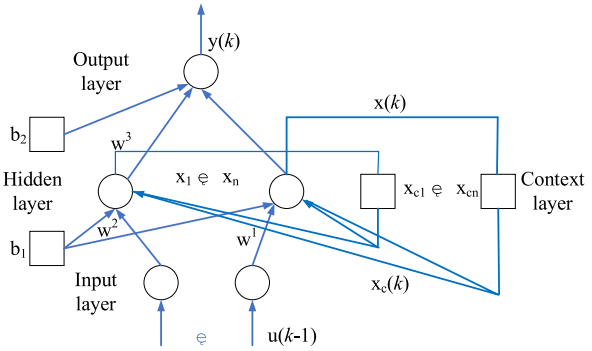

FIGURE 9. Structure of Elman neural network.

From Fig.9, the nonlinear state space function of the Elman NN can be expressed as

$$\begin{cases} y(k) = g(\omega^3 x(k)) \\ x(k) = f(\omega^1 x_c(k) + \omega^2(u(k-1))) \\ x_c(k) = x(k-1) \end{cases} \tag{16}$$

where is the m-dimensional vector of output layer, x is the n-dimensional mid-layer node vector, u is the r-dimensional

vector of input layer, x_c is an n-dimensional feedback state vector. ω^3, ω^2 and ω^1 are the corresponding weight matrixes among the output layer, middle layer, input layer, and context layer, respectively. g is the transfer function of the output neuron, and f is the transfer function of neurons in the middle layer.

The sum of error squares is adopted as the learning indicator, then the total error criterion function for training samples can be calculated,

$$E = \frac{1}{2}\sum_{k=1}^{n}(y(k) - \tilde{y}(k))^2 \tag{17}$$

where $y(k)$ is the expected output and $\tilde{y}(k)$ is the predicted output. According to the error gradient descent method, we can attain:

$$\Delta\omega = -\eta\frac{\partial E}{\partial \omega} \tag{18}$$

Then, the modified connection weight can be calculated,

$$\begin{cases} \Delta\omega_{ij}^3 = -\eta_3\dfrac{\partial E}{\partial \omega_{ij}^3} & i = 1, 2, \cdots, m;\ j = 1, 2, \cdots, n \\ \Delta\omega_{jh}^2 = -\eta_2\dfrac{\partial E}{\partial \omega_{jh}^2} & h = 1, 2, \cdots, r \\ \Delta\omega_{jq}^1 = -\eta_1\dfrac{\partial E}{\partial \omega_{jq}^1} & q = 1, 2, \cdots, n \end{cases} \tag{19}$$

where η_1, η_2 and η_3 are the learning rates of ω^1, ω^2 and ω^3, respectively. In addition, we can further get:

$$\frac{\partial E}{\partial \omega_{ij}^3} = \frac{\partial E}{\partial \tilde{y}_i(k)}\frac{\partial \tilde{y}_i(k)}{\partial g_i(*)}\frac{\partial g_i(*)}{\partial \omega_{ij}^3} \tag{20}$$

From (16) and (17), we can attain:

$$\frac{\partial E}{\partial \omega_{ij}^3} = \frac{\partial E}{\partial \tilde{y}_i(k)}g_i'(*)x_j(k) \tag{21}$$

$$\frac{\partial E}{\partial \tilde{y}_i(k)} = -\sum_{k=1}^{n}(y_i(k) - \tilde{y}_i(k)) \tag{22}$$

$$\frac{\partial E}{\partial \omega_{ij}^3} = -\sum_{k=1}^{n}(y_i(k) - \tilde{y}_i(k))g_i'(*)x_j(k) \tag{23}$$

Meanwhile, partial derivative of ω_{jh}^2 can be described as:

$$\frac{\partial E}{\partial \omega_{jh}^2} = \frac{\partial E}{\partial x_j(k)}\frac{\partial x_j(k)}{\partial \omega_{jh}^2} = \frac{\partial E}{\partial x_j(k)}f_j'(*)u_h(k-1) \tag{24}$$

Since

$$\frac{\partial E}{\partial x_j(k)} = \frac{\partial E}{\partial \tilde{y}_i(k)}\frac{\partial \tilde{y}_i(k)}{\partial x_j(k)} = \frac{\partial E}{\partial \tilde{y}_i(k)}g'(*)\omega_j^3 \tag{25}$$

we can get

$$\begin{cases} \dfrac{\partial E}{\partial \omega_{jh}^2} = -\displaystyle\sum_{k=1}^{n}(y_i(k) - \tilde{y}_i(k))g'(*)\omega_j^3 f_j'(*)u_h(k-1) \\ \dfrac{\partial E}{\partial \omega_{ij}^1} = -\displaystyle\sum_{k=1}^{n}(y_i(k) - \tilde{y}_i(k))g'(*)\omega_j^3 f_j'(*)x_{c,q}(k) \end{cases} \tag{26}$$

Assuming that

$$\sum_{k=1}^{n}(y_i(k) - \tilde{y}_i(k)) = \zeta_i^j \tag{27}$$

we can obtain:

$$\begin{cases} \Delta\omega_{ij}^3 = \eta_3\zeta_i^j g_i'(*)x_j(k) \\ \qquad i = 1, 2, \cdots, m;\ j = 1, 2, \cdots, n \\ \Delta\omega_{jh}^2 = \eta_2\zeta_i^j g'(*)\omega_j^3 f_j'(*)u_h(k-1) \\ \qquad h = 1, 2, \cdots, r \\ \Delta\omega_{jq}^1 = \eta_1\zeta_i^j g'(*)\omega_j^3 f_j'(*)x_{c,q}(k) \\ \qquad q = 1, 2, \cdots, n \end{cases} \tag{28}$$

Next step, the results analysis and prediction precision are discussed with the proposed algorithm.

V. PREDICTED RESULTS AND ANALYSIS

As can be seen from Figs. 5 and 6, the SOH curves of two batteries are obviously different. The local capacity recovery of Cell 2 is more obvious and the available capacity drops fasters than that of Cell 1. From Figs. 5 and 6 (a), we can find that the oscillation amplitude and frequency of IMFs are obviously different, and different prediction effects would be obtained after the ARMA model prediction. For the residue, due to the large difference in cycle numbers of life attenuation experiments, the amount of data used for training differs greatly when the Elman NN is employed, and thus different prediction results are generated. In this study, the mean-square error (MSE) and mean-absolute-relative error (MARE) are employed to quantitatively evaluate the prediction results, as:

$$MSE = \frac{1}{N}\sum_{i=1}^{N}(f(x_i) - y_i)^2 \tag{29}$$

$$MARE = \frac{1}{N}\sum_{i=1}^{N}\frac{|f(x_i) - y_i|}{y_i} \times 100\% \tag{30}$$

where N is the number of samples, $f(x_i)$ is the predicted value of the samples, and y_i is the referred value of the samples. The MSE is mainly to describe the influences of the sample with large errors, and the MARE is used to quantify the average error of the model. In this study, the prediction effect of IMFs and residue for two batteries are compared and discussed. Finally, the SOH prediction results of the two batteries are compared with that only based on a single ARMA model and the Elman NN.

A. ESTIMATION RESULTS OF IMFS AND RESIDUE

The results predicted of IMFs and residue for two cells by the proposed model are shown in Figs. 10 to 13, and the comprehensive prediction errors of IMF1, IMF2 and IMF3 are depicted in TABLE 5. The MSE and MARE of IMFs for Cell 1 predicted by the ARMA algorithm are $0.17\times10\text{-}5^{-}$ and 2.16%, respectively. The error performance of residue for Cell 1 predicted by the Elman NN are $0.69\times10\text{-}5^{-}$ and 0.18%. For Cell 2, the indexes describing

TABLE 5. Error comparison of IMFs and residue.

Item	Cell 1		Cell 2	
	MSE (10^{-5})	MARE (%)	MSE (10^{-5})	MARE (%)
IMFs	0.17	2.16	3.79	6.83
residue	0.69	0.18	6.50	0.51

the prediction performance are 3.79×10-5−, 6.83% of IMFs and 6.50×10-5−, 0.51% of residue, respectively. As can be seen in TABLE 5, the MSE of IMFs predicted by ARMA is smaller than the residue predicted by Elman NN, while the MARE of IMFs predicted by ARMA is higher than the MARE predicted by Elman NN. This is due to the different performance of the two models. However, both models can achieve desirable prediction accuracy. To sum up, we can conclude that the ARMA model and Elman NN are capable of tracking the signal variation with high accuracy.

B. SOH ESTIMATION RESULTS OF TWO BATTERIES

As shown in Part A, the prediction performance of both methods is validated effective. In this paper, the prediction results of IMFs and residue are added together to predict the SOH. The results predicted are shown in Figs. 14 and 15, including the prediction results and errors. For Cell 1, most of the absolute error can be guaranteed within 1%, and the distribution is relatively concentrated. The large prediction error of Cell 1 is caused by the presence of individual outliers in the extracted health factor F1. For Cell 2, the overall absolute error is restricted within 2%, however, when comparing with that of Cell 1, the error distribution is relatively dispersed, which is raised by the large local oscillation of the SOH. As can be seen from Figs. 14 and 15, in the whole cycle life experiment of Cell 1, its SOH is always greater than 80%. However, for Cell 2, when the SOH is below 80% after 120 cycles, its capacity dropped more rapidly. The maximum prediction error for Cell 1 is kept within 0.5%, and when the SOH of Cell 2 locates within 80% to 100%, most of the estimation error is less than 1.5%. Even there exists a large oscillation in the end of the prediction error distribution profile, however, the maximum prediction error is still less than 3%. Therefore, we can conclude that the proposed method is capable of estimating the battery SOH with satisfactory precision. To sum up, the fusion algorithm can ensure high estimation precision and results manifest that the algorithm can effectively predict the SOH by dealing with the local information variation and extracting the healthy indicator after consideration of the battery polarization.

C. COMPARISON OF THE SOH ESTIMATION RESULTS

To verify the prediction performance and conformability of the fusion model, the single ARMA model and the Elman NN prediction are also employed for performance comparison.

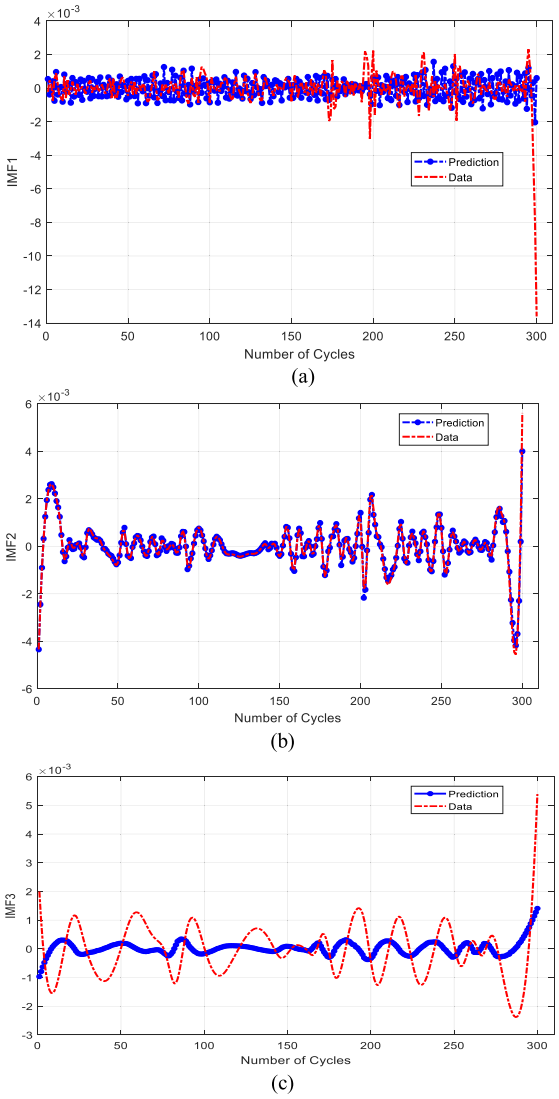

FIGURE 10. Results of IMFs estimation by the ARMA for Cell 1. (a) IMF1 estimation results. (b) IMF2 estimation results. (c) IMF3 estimation results.

Figs. 16 to 21 and TABLE 6 show the prediction results and errors of the ARMA model and Elman NN, respectively.

For Cell 1, the MSE and MARE based on these three methods, i.e., the fusion algorithm, ARMA model and Elman NN method are 0.94 × 10−− and 0.21%, 0.13 × 10 − 5− and 0.08%, and 2.95 × 10 − 5− and 0.41%, respectively. Among them, the prediction error of the Elman NN algorithm is larger than that of the ARMA-Elman NN algorithm, and the prediction error of the ARMA model is smaller than that of the fusion model. The SOH variation of Cell 1 is relatively smooth without much fluctuation in the middle part and the ARMA model requires a higher level of stability for the predicted data. The IMFs obtained by the EMD represent the local frequency amplitude, the fluctuation of the IMF result is larger than that of the SOH sequence. Therefore, the error of SOH directly predicted by the ARMA model will be small.

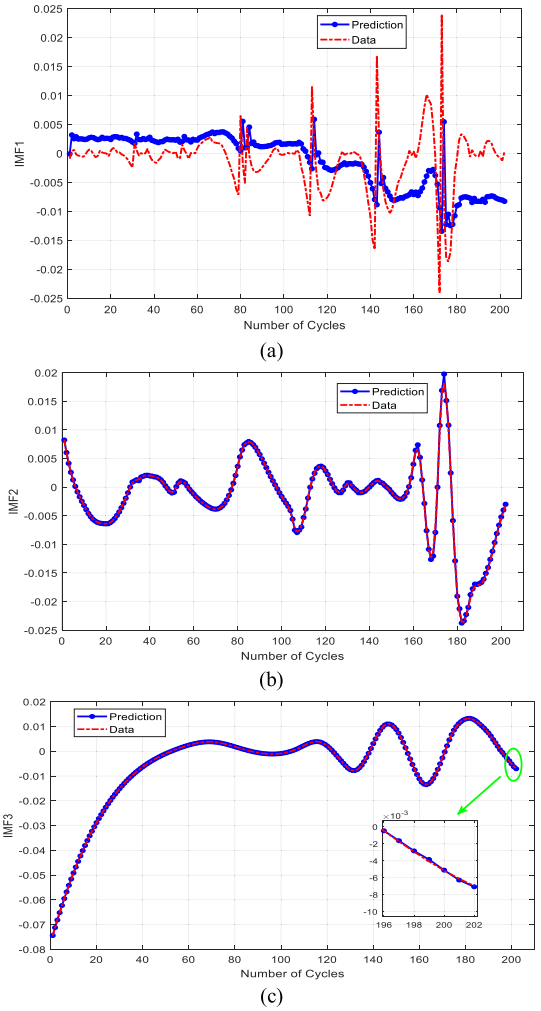

FIGURE 11. Results of IMFs estimation by the ARMA for Cell 2. (a) IMF1 estimation results. (b) IMF2 estimation results. (c) IMF3 estimation results.

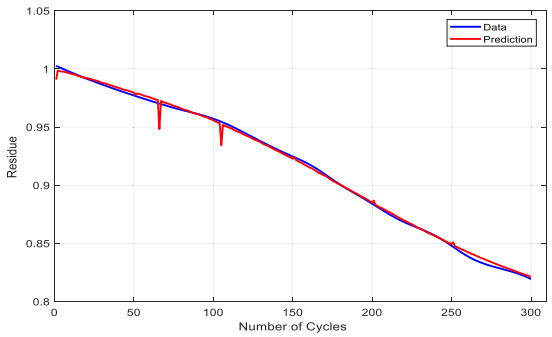

FIGURE 12. Results of residue estimation by the Elman NN for Cell 1.

However, the disadvantage of the ARMA model is that it cannot specifically consider the correlation among battery aging features, such as F1 and SOH, therefore, the prediction results may not be comprehensive.

For Cell 2, the corresponding results are $7.20 \times 10 - 5^{-}$ and 0.72%, $9.20 \times 10 - 5^{-}$ and 0.64%, and $8.70 \times 10 - 5^{-}$

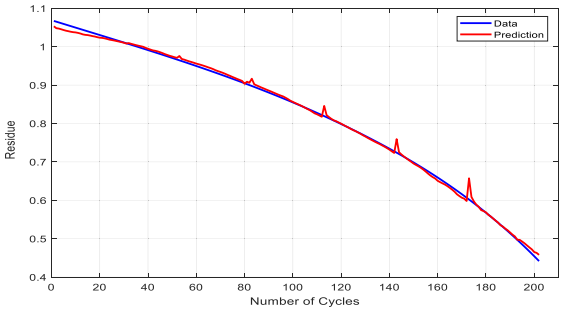

FIGURE 13. Results of residue estimation by the Elman NN for Cell 2.

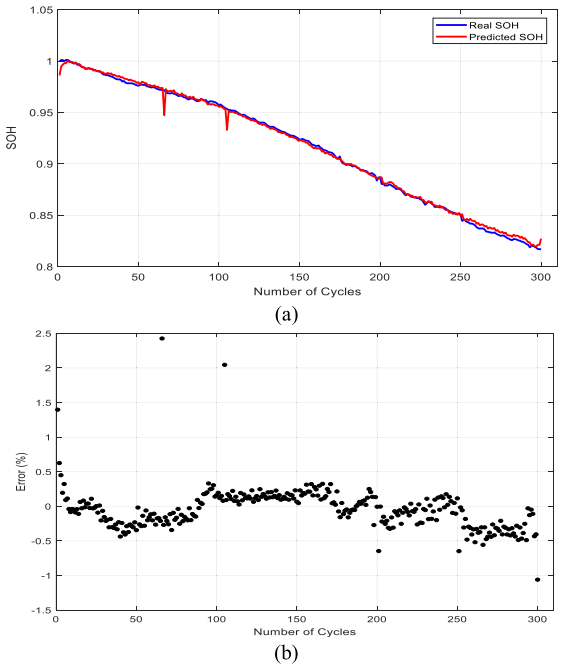

FIGURE 14. The results and error of SOH estimation for Cell 1.

and 0.60%, respectively. As can be observed, the prediction errors of these three methods are relatively close, the MSE of the fusion model is smaller than that of the ARMA and Elman NN, whereas the MARE is slightly larger. When the Elman NN predicts the data sequence that has a large correlation with past observation, the prediction performance is not as ideal as the ARMA model; in contrast, the Elman NN can consider the mapping between the aging factor and the SOH. To conclude, the fusion method can not only consider more comprehensive information change during the prediction, but also ensure high estimation accuracy by incorporating the advantages of the ARMA and Elman NN. As such, we can say that the proposed fusion method demonstrates higher application potential in the actual process.

D. STATE OF HEALTH ESTIMATION FOR DIFFERENT CELLS

To further validate feasibility of the proposed method, another three cells, i.e., Cells 3, 4, and 5, are experimented on. Cells 3 and 4 belong to the same type as Cell 1, and Cell 5 is

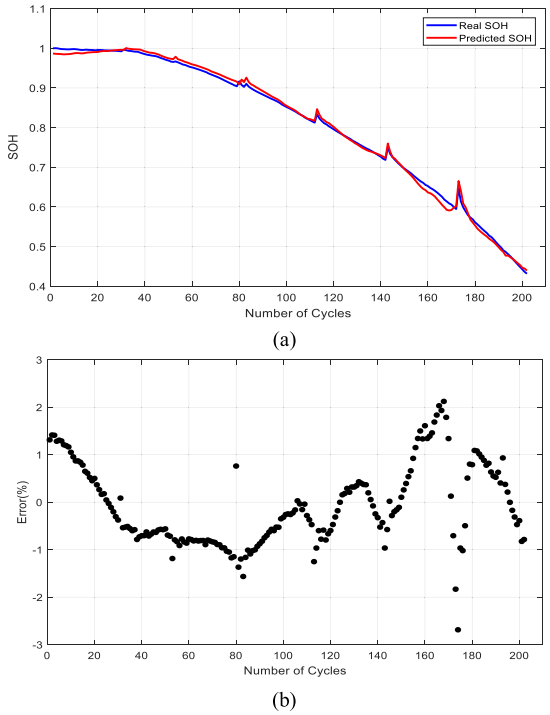

FIGURE 15. The results and error of SOH estimation for Cell 2.

TABLE 6. Comparison of SOH prediction error for Cell 1 and Cell 2.

Method	Battery number	MSE(10^{-5})	MARE(%)
ARMA-Elman NN	Cell 1	0.94	0.21
	Cell 2	7.20	0.72
Elman NN	Cell 1	2.95	0.41
	Cell 2	8.70	0.60
ARMA	Cell 1	0.13	0.08
	Cell 2	9.20	0.64

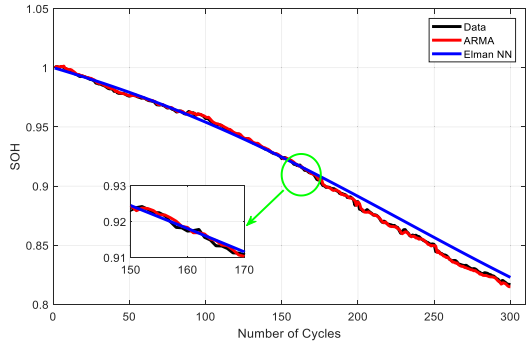

FIGURE 16. Estimation Results by ARMA and Elman NN for Cell 1.

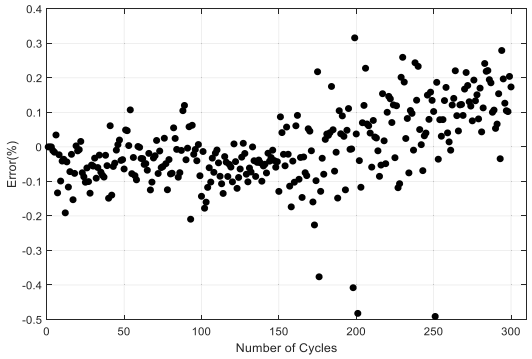

FIGURE 17. Estimation error of the SOH by ARMA for Cell 1.

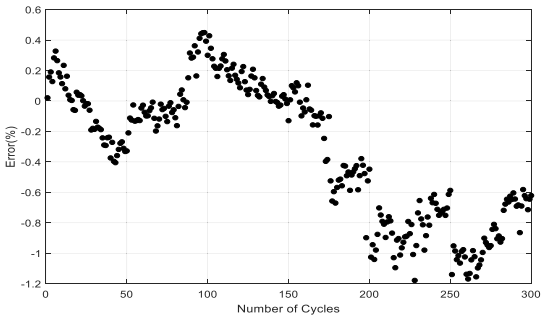

FIGURE 18. Estimation error of the SOH by Elman NN for Cell 1.

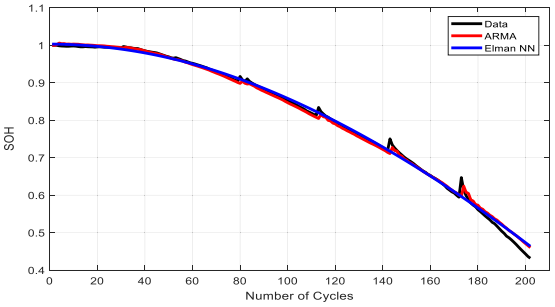

FIGURE 19. SOH estimation results by ARMA and Elman NN for Cell 2.

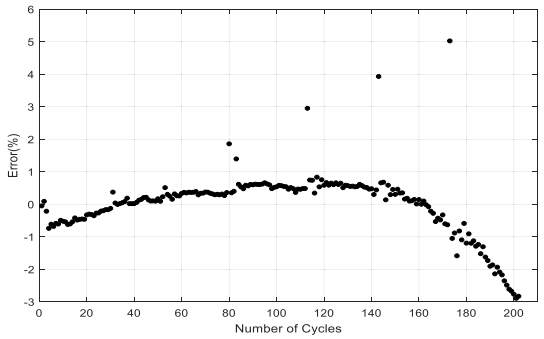

FIGURE 20. Estimation error of the SOH by ARMA for Cell 2.

the same with Cell 2. Their predictions and errors are shown in Figs. 22 to 24 and TABLE 7. We need to point out that since the rest occurs intermittently during the experiment of Cell 4, its capacity decline is not obvious. It can be seen that the proposed method can attain a small prediction error, of which the MSE and MARE for these three Cells are $1.2 \times 10 - 5^{-}$, $1.90 \times 10 - 5^{-}$, $9.20 \times 10 - 5^{-}$, and 0.27%, 0.37%, 0.57%, respectively. As the SOH of Cell 5 drops far less than 80% at the end of cycle life, the estimation error

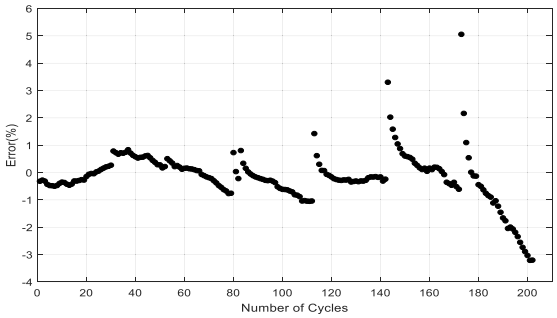

FIGURE 21. Estimation error of the SOH by Elman NN for Cell 2.

TABLE 7. Comparison of SOH prediction error for Cells 3 to 5.

Error	Cell 3	Cell 4	Cell 5
MSE(10^{-5})	1.2	1.9	9.2
MARE(%)	0.27	0.37	0.57

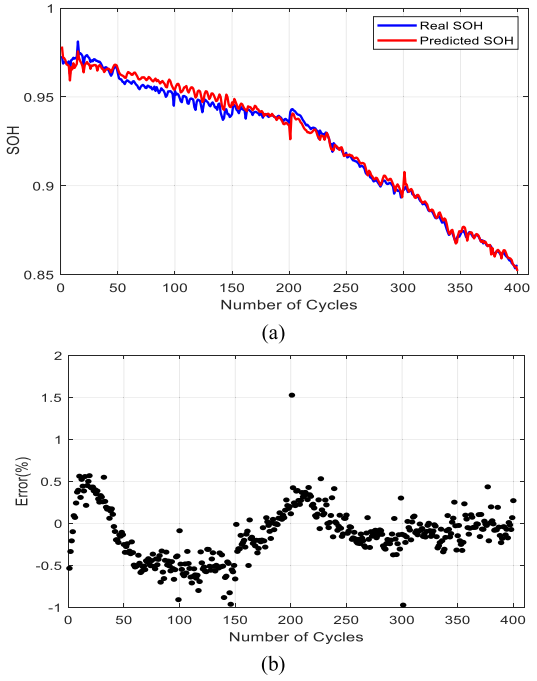

FIGURE 22. The results and error of SOH estimation for Cell 3.

of Cell 5 gradually increases. By comparing with the results of Cell 2, we can find that the algorithm leads to the similar performance as Cell 2, proving that our method can conduct the consistent prediction for one type of cells. We can find that the absolute prediction error of all batteries is almost the same, and the error distribution is relatively concentrated, manifesting the effectiveness of the algorithm when applied to different batteries.

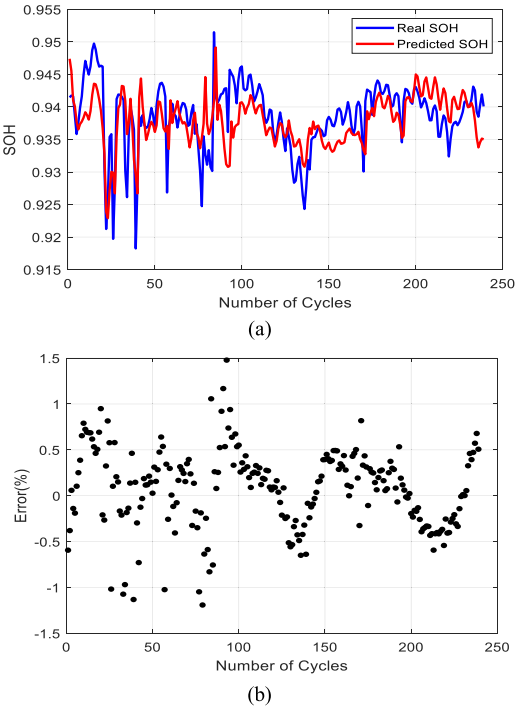

FIGURE 23. The results and error of SOH estimation for Cell 4.

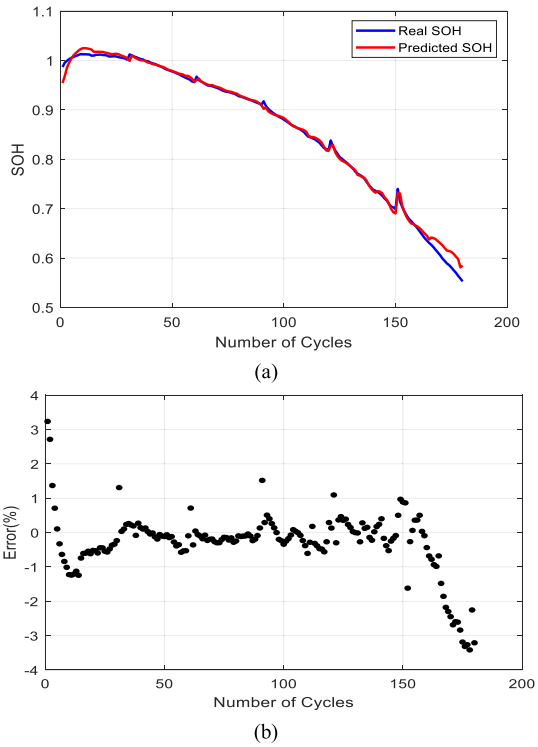

FIGURE 24. The results and error of SOH estimation for Cell 5.

E. VERIFICATION OF METHOD ROBUSTNESS

All the above discussed results are obtained under a deterministic way of charging/discharging the battery. To prove robustness of the proposed method, an open source battery

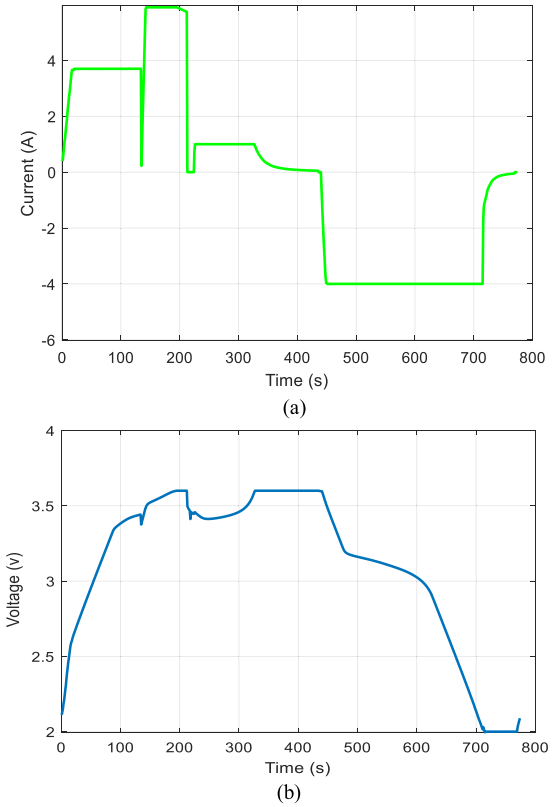

FIGURE 25. Current and Voltage change during a cycle for Cell 6.

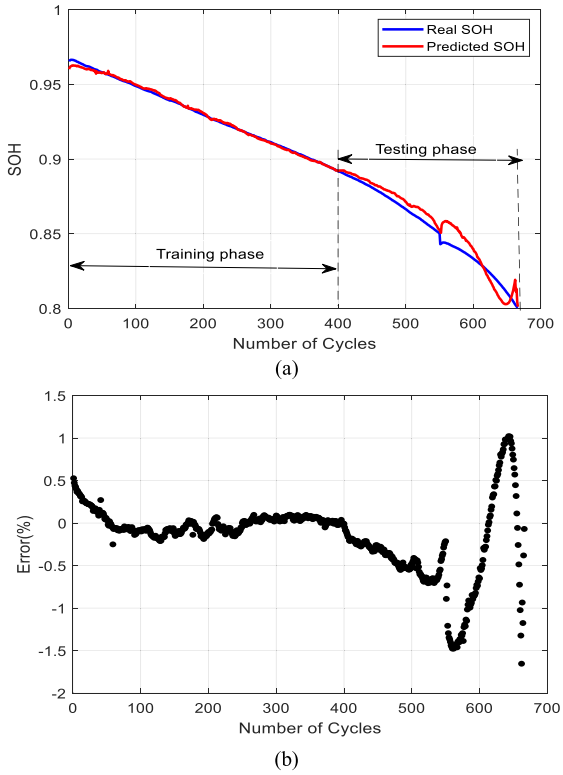

FIGURE 26. The results and error of SOH estimation for Cell 6.

experimental data is selected for extended verification. The open data set was collected by cyclic life tests of a variety of commercial LFP/graphite batteries (rated capacity of 1.1Ah and rated voltage of 3.3V). Some experiments adopt one-step or two-step policy to charge the battery, and the upper and lower cut-off voltages are 3.6 V and 2.0 V, respectively. The charging policy that we select specifies a format of C1(Q1)-C2 mode, in which C1 and C2 denote the first and second constant current step, respectively, and Q1 is the SOC at which the current changes. The second current step ends at 80% SOC, after that the cell is charged with 1C CC-CV mode. More details can be found in [28]. To extend the validation, the experimental data of one battery, referred to Cell 6, is selected to verify the proposed method.

Fig. 25 shows the current and voltage variation in a charging and discharging cycle. It can be seen that the current varies dramatically in the charging process, and the charging mode is not a determined manner. We extend the feature selection range for Cell 6 and extract the whole charging time as a health factor. Then, the proposed algorithm is applied to predict the SOH. The estimation result and error are shown in Fig. 26. As can be observed, the estimation result shows similar trend with the real SOH, and only some fluctuation exists when the SOH is close to 80%. As a result, a conclusion can be made that the overall prediction error is less than 1.5%, and all the test results are within a reasonable error range. In this manner, the robustness and adaptivity of the proposed algorithm is proved.

VI. CONCLUSION

In this paper, a fusion state of health estimation algorithm is proposed based on the autoregressive moving average model and the Elman neural network algorithm. To achieve state of health estimation, the charging and discharging voltage curve and capacity variation of five lithium-ion batteries, are acquired from the experimental data. The constant current mode charging duration is extracted as the health factor according to changing characteristics of the voltage curve during the charging process. Secondly, the raw state of health sequence is processed by the empirical mode decomposition to acquire three intrinsic mode functions together with a residue. The grey relational analysis of intrinsic mode functions and the residue with the health factor and cycle numbers are conducted. Different prediction models are selected according to the calculated correlation grade. Among them, intrinsic mode functions, which show high correlation with historical observations, are predicted by the autoregressive moving average model, and the residue, which are strongly correlated with the health factor and cycle numbers, are predicted by the Elman neural network. Meanwhile, all the predicted values are added together to determine the state of health. Comparing with the results calculated only based on the autoregressive moving average model and the Elman neural network algorithm, experimental results manifest that the

proposed fusion algorithm can not only consider the influence of complex changes on state of health, but also ensure a high prediction accuracy.

In the next step, the influence of other factors that can take an effect in the SOH estimation should be studied, such as temperature variation, different charge and discharge rates, and variation of external operating environment. In addition, conduction of the SOH estimation based only on partial charging duration in the CC mode will be our research direction. Currently, we do not specifically consider the battery capacity decline in some extreme conditions, which will also be our next research content for extending the application of the algorithm. Furthermore, this paper only studies the SOH of the single battery cell and the investigation of the pack SOH could also be our research focus in the future.

REFERENCES

[1] L. Cai, J. H. Meng, D. I. Stroe, G. Z. Luo, and R. Teodorescu, "An evolutionary framework for lithium-ion battery state of health estimation," *J. Power Sources*, vol. 412, pp. 615–622, Feb. 2019.

[2] X. Li, Z. Wang, L. Zhang, C. Zou, and D. Dorrell, "State-of-health estimation for Li-ion batteries by combing the incremental capacity analysis method with grey relational analysis," *J. Power Sources*, vols. 410–411, pp. 106–114, Jan. 2019.

[3] Y. Li, S. Zhong, Q. Zhong, and K. Shi, "Lithium-ion battery state of health monitoring based on ensemble learning," *IEEE Access*, vol. 7, pp. 8754–8762, Jan. 2019.

[4] M. Galeotti, C. Giammanco, L. Ciná, S. Cordiner, and A. Di Carlo, "Synthetic methods for the evaluation of the state of health (SOH) of nickel-metal hydride (NiMH) batteries," *Energy Convers. Manage.*, vol. 92, pp. 1–9, Mar. 2015.

[5] L. D. Couto, J. Schorsch, N. Job, A. Léonard, and M. Kinnaert, "State of health estimation for lithium ion batteries based on an equivalent-hydraulic model: An iron phosphate application," *J. Energy Storage*, vol. 21, pp. 259–271, Feb. 2019.

[6] Z. Wang, J. Ma, and L. Zhang, "State-of-health estimation for lithium-ion batteries based on the multi-Island genetic algorithm and the Gaussian process regression," *IEEE Access*, vol. 5, pp. 21286–21295, 2017.

[7] R. Xiong, J. Tian, H. Mu, and C. Wang, "A systematic model-based degradation behavior recognition and health monitoring method for lithium-ion batteries," *Appl. Energy*, vol. 207, pp. 372–383, Dec. 2017.

[8] Y. Zhou and M. Huang, "Lithium-ion batteries remaining useful life prediction based on a mixture of empirical mode decomposition and ARIMA model," *Microelectron. Rel.*, vol. 65, pp. 265–273, Oct. 2016.

[9] A. Barré, B. Deguilhem, S. Grolleau, M. Gérard, F. Suard, and D. Riu, "A review on lithium-ion battery ageing mechanisms and estimations for automotive applications," *J. Power Sour.*, vol. 241, pp. 680–689, Nov. 2013.

[10] C. Weng, X. Feng, J. Sun, and H. Peng, "State-of-health monitoring of lithium-ion battery modules and packs via incremental capacity peak tracking," *Appl. Energy*, vol. 180, pp. 360–368, Oct. 2016.

[11] Y. Li, M. A. Monem, R. Gopalakrishnan, M. Berecibar, E. N. Maury, N. Omar, P. Bossche, and J. V. Mierlo, "A quick on-line state of health estimation method for Li-ion battery with incremental capacity curves processed by Gaussian filter," *J. Power Sources*, vol. 373, pp. 40–53, Jan. 2018.

[12] Z. Ma, R. Yang, and Z. Wang, "A novel data-model fusion state-of-health estimation approach for lithium-ion batteries," *Appl. Energy*, vol. 237, pp. 836–847, Mar. 2019.

[13] D. Yang, X. Zhang, R. Pan, Y. Wang, and Z. Chen, "A novel Gaussian process regression model for state-of-health estimation of lithium-ion battery using charging curve," *J. Power Sour.*, vol. 384, pp. 387–395, Apr. 2018. doi: 10.1016/j.jpowsour.2018.03.015.

[14] G. Giordano, V. Klass, M. Behm, G. Lindbergh, and J. Sjöberg, "Model-based lithium-ion battery resistance estimation from electric vehicle operating data," *IEEE Trans. Veh. Technol.*, vol. 67, no. 5, pp. 3720–3728, May 2018.

[15] J. Du, Z. Liu, Y. Wang, and C. Wen, "An adaptive sliding mode observer for lithium-ion battery state of charge and state of health estimation in electric vehicles," *Control Eng. Pract.*, vol. 54, pp. 81–90, Sep. 2016.

[16] J. Li, K. Adewuyi, N. Lotfi, R. G. Landers, and J. Park, "A single particle model with chemical/mechanical degradation physics for lithium ion battery state of health (SOH) estimation," *Appl. Energy*, vol. 212, pp. 1178–1190, Feb. 2018.

[17] Y. Zou, X. Hu, H. Ma, and S. E. Li, "Combined state of charge and state of health estimation over lithium-ion battery cell cycle lifespan for electric vehicles," *J. Power Sour.*, vol. 273, pp. 793–803, Jan. 2015.

[18] C. Hametner, S. Jakubek, and W. Prochazka, "Data-driven design of a cascaded observer for battery state of health estimation," *IEEE Trans. Ind. Appl.*, vol. 54, no. 6, pp. 6258–6266, Nov./Dec. 2018.

[19] R. Xiong, F. Sun, Z. Chen, and H. He, "A data-driven multi-scale extended Kalman filtering based parameter and state estimation approach of lithium-ion polymer battery in electric vehicles," *Appl. Energy*, vol. 113, pp. 463–476, Jan. 2014.

[20] Z. Chen, M. Sun, X. Shu, R. Xiao, and J. Shen, "Online state of health estimation for lithium-ion batteries based on support vector machine," *Appl. Sci.-Basel*, vol. 8, no. 6, Jun. 2018, Art. no. 925.

[21] V. Klass, M. Behm, and G. Lindbergh, "A support vector machine-based state-of-health estimation method for lithium-ion batteries under electric vehicle operation," *J. Power Sources*, vol. 270, pp. 262–272, Dec. 2014.

[22] J. Wu, Y. J. Wang, X. Zhang, and Z. H. Chen, "A novel state of health estimation method of Li-ion battery using group method of data handling," *J. Power Sources*, vol. 327, pp. 457–464, Sep. 2016.

[23] D. Zhou, H. T. Yin, P. Fu, X. H. Song, W. B. Lu, L. L. Yuan, and Z. X. Fu, "Prognostics for state of health of lithium-ion batteries based on Gaussian process regression," *Math. Problems Eng.*, vol. 11, Apr. 2018, Art. no. 8358025.

[24] Y. Song, D. Liu, C. Yang, and Y. Peng, "Data-driven hybrid remaining useful life estimation approach for spacecraft lithium-ion battery," *Microelectron. Rel.*, vol. 75, pp. 142–153, Aug. 2017.

[25] Y. Li, C. F. Zou, M. Berecibar, E. Elise Nanini, J. C. W. Chan, P. van den Bossche, J. Van Mierlo, and N. Omar, "Random forest regression for online capacity estimation of lithium-ion batteries," *Appl. Energy, Article*, vol. 232, pp. 197–210, Dec. 2018.

[26] Z. Wang, S. Zeng, J. Guo, and T. Qin, "State of health estimation of lithium-ion batteries based on the constant voltage charging curve," *Energy*, vol. 167, pp. 661–669, Jan. 2019.

[27] P. Y. Guo, Z. Cheng, and L. Yang, "A data-driven remaining capacity estimation approach for lithium-ion batteries based on charging health feature extraction," *J. Power Sources*, vol. 412, pp. 442–450, Feb. 2019.

[28] A. K. Severson, M. P. Attia, N. Jin, N. Perkins, B. Jiang, and Z. Yang, "Data-driven prediction of battery cycle life before capacity degradation," *Nature Energy*, vol. 4, no. 5, pp. 383–391, May 2019.

[29] X. Li, Z. Wang, and J. Yan, "Prognostic health condition for lithium battery using the partial incremental capacity and Gaussian process regression," *J. Power Sources*, vol. 421, pp. 56–67, May 2019.

[30] R. Xiong, L. Li, and J. Tian, "Towards a smarter battery management system: A critical review on battery state of health monitoring methods," *J. Power Sources*, vol. 405, pp. 18–29, Nov. 2018.

[31] X. Zhang, Y. Wang, C. Liu, and Z. Chen, "A novel approach of battery pack state of health estimation using artificial intelligence optimization algorithm," *J. Power Sources*, vol. 376, pp. 191–199, Feb. 2018.

[32] B. E. Olivares, M. A. Cerda Muñoz, M. E. Orchard, and J. F. Silva, "Particle-filtering-based prognosis framework for energy storage devices with a statistical characterization of state-of-health regeneration phenomena," *IEEE Trans. Instrum. Meas.*, vol. 62, no. 2, pp. 364–376, Feb. 2013.

[33] L. Xue, J. Jiang, Y. W. Le, D. Chen, Y. Zhang, and C. J. A. E. Zhang, "A capacity model based on charging process for state of health estimation of lithium ion batteries," *Appl. Energy*, vol. 177, pp. 537–543, Sep. 2016.

[34] W. Waag, S. Käbitz, and D. U. Sauer, "Experimental investigation of the lithium-ion battery impedance characteristic at various conditions and aging states and its influence on the application," *Appl. Energy*, vol. 102, no. 2, pp. 885–897, 2013.

[35] D. Liu, J. Zhou, H. Liao, Y. Peng, and X. Peng, "A health indicator extraction and optimization framework for lithium-ion battery degradation modeling and prognostics," *IEEE Trans. Syst., Man, Cybern. Syst*, vol. 45, no. 6, pp. 915–928, Jun. 2015.

[36] J. Feng, P. Kvam, and Y. Tang, "Remaining useful lifetime prediction based on the damage-marker bivariate degradation model: A case study on lithium-ion batteries used in electric vehicles," *Eng. Failure Anal.*, vol. 70, pp. 323–342, Dec. 2016.

[37] L. Wang, C. Pan, L. Liu, Y. Cheng, and X. Zhao, "On-board state of health estimation of $LiFePO_4$ battery pack through differential voltage analysis," *Appl. Energy*, vol. 168, pp. 465–472, Apr. 2016.
[38] M. H. Lipu, M. A. Hannan, A. Hussain, M. M. Hoque, P. J. Ker, M. H. M. Saad, and F. Ayob, "A review of state of health and remaining useful life estimation methods for lithium-ion battery in electric vehicles: Challenges and recommendations," *J. Cleaner Prod.*, vol. 205, pp. 115–133, Dec. 2018.
[39] N. E. Huang, Z. Shen, S. R. Long, M. C. Wu, H. H. Shih, Q. Zheng, N. C. Yen, C. C. Tung, and H. H. Liu, "The empirical mode decomposition and the Hilbert spectrum for nonlinear and non-stationary time series analysis," *Proc. Roy. Soc. London Ser. A, Math., Phys. Eng. Sci.*, vol. 454, no. 1971, pp. 903–995, Mar. 1998.
[40] H. Liu, H. Q. Tian, and Y. F. Li, "Comparison of new hybrid FEEMD-MLP, FEEMD-ANFIS, wavelet packet-MLP and wavelet packet-ANFIS for wind speed predictions," *Energy Convers. Manage.*, vol. 89, pp. 1–11, Jan. 2015.
[41] A. O. Boudraa and J. C. Cexus, "EMD-based signal filtering," *IEEE Trans. Instrum. Meas.*, vol. 56, no. 6, pp. 2196–2202, Dec. 2007.
[42] P. Wang, P. Meng, and B. Song, "Response surface method using grey relational analysis for decision making in weapon system selection," *J. Syst. Eng. Electron.*, vol. 25, no. 2, pp. 265–272, Apr. 2014.
[43] D. Faranda, F. M. E. Pons, B. Dubrulle, F. Daviaud, B. Saint-Michel, E. Herbert, and P. P. Cortet, "Modelling and analysis of turbulent datasets using auto regressive moving Average processes," *Phys. Fluids, Article*, vol. 26, no. 10, Oct. 2014, Art. no. 105101.
[44] S. Dilling and B. J. MacVicar, "Cleaning high-frequency velocity profile data with autoregressive moving average (ARMA) models," *Flow Meas. Instrum.*, vol. 54, pp. 68–81, Apr. 2017.
[45] K. Kimura and H. Waki, "Minimization of Akaike's information criterion in linear regression analysis via mixed integer nonlinear program," *Optim. Methods Softw.*, vol. 33, no. 3, pp. 633–649, Jun. 2018.
[46] T. Cassar, K. P. Camilleri, and S. G. Fabri, "Order estimation of multivariate ARMA models," *IEEE J. Sel. Topics Signal Process.*, vol. 4, no. 3, pp. 494–503, Jun. 2010.
[47] K. P. Jayalath, H. K. T. Ng, A. B. Manage, and K. E. Riggs, "Improved tests for homogeneity of variances," *Commun. Statist.-Simul. Comput.*, vol. 46, no. 9, pp. 7423–7446, Oct. 2017.
[48] W. Z. Sun and J. S. Wang, "Elman neural network soft-sensor model of conversion velocity in polymerization process optimized by chaos whale optimization algorithm," *IEEE Access*, vol. 5, pp. 13062–13076, 2017.
[49] H. Liu, H.-Q. Tian, X. Liang, and Y.-F. Li, "Wind speed forecasting approach using secondary decomposition algorithm and Elman neural networks," *Appl. Energy*, vol. 157, pp. 183–194, Nov. 2015.

ZHENG CHEN received the B.S. and M.S. degrees in electrical engineering and the Ph.D. degree in control science engineering from Northwestern Polytechnical University, Xi'an, China, in 2004, 2007, and 2012, respectively.

He is currently a Professor with the Faculty of Transportation Engineering, Kunming University of Science and Technology, Kunming, Yunnan, China. He was a Postdoctoral Fellow and a Research Scholar with the University of Michigan, Dearborn, MI, USA, from 2008 to 2014. His research interests include battery management systems, battery status estimation, and energy management of hybrid electric vehicles. He has conducted more than 20 projects and has published more than 80 peer-reviewed journal papers and conference proceedings. He is the receiver of the Yunnan Oversea High Talent Project, China, and the second place of the IEEE VTS Motor Vehicles Challenge, in 2017 and 2018, respectively.

QIAO XUE received the B.S. degrees in traffic engineering from the Kunming University of Science and Technology, Kunming, China, in 2018, where he is currently pursuing the M.S. degrees in transportation engineering.

His research interests include state of health monitoring for battery and battery management systems.

RENXIN XIAO received the B.S., M.S., and Ph.D. degrees in automation, control theory and control engineering, and mechanical design and theory from the Kunming University of Science and Technology, Kunming, China, in 2003, 2006, and 2013, respectively.

From 2006 to 2009, he worked for servo control as an Engineer with the Kunming Institute of Physics, Kunming. He is currently an Associate Professor with the Faculty of Transportation Engineering, Kunming University of Science and Technology, Kunming. His research interests include modeling of electric vehicle, battery management systems, and servo control of motor.

YONGGANG LIU received the B.S. and Ph.D. degrees in automotive engineering from Chongqing University, Chongqing, China, in 2004 and 2010, respectively. He was a joint Ph.D. student and a Research Scholar with the University of Michigan-Dearborn, MI, USA, from 2007 to 2009.

He is currently a Professor and the Dean Assistant with the School of Automotive Engineering, Chongqing University. His research interests mainly include optimization and control of intelligent electric and hybrid vehicles, and integrated control of vehicle automatic transmission systems. He has lead more than 10 research projects, and has published more than 40 research journal papers. He is also a committee member of the Vehicle Control and Intelligence Society of the Chinese Association of Automation (CAA).

JIANGWEI SHEN received the B.S. and M.S. degrees in traffic engineering, and power machine and engineering from the Kunming University of Science and Technology, Kunming, China, in 2008 and 2011, respectively. He is currently pursuing the Ph.D. degree in automobile engineering with the Kunming University of Science and Technology, where he is currently an Experimentalist.

His research interests include battery management systems and energy management of hybrid electric vehicles.